AIAA JOURNAL
Vol. 49, No. 5, May 2011

Hyperbolic Algorithm for Coupled Plasma/Electromagnetic Fields Including Conduction and Displacement Currents

D. Li* and C. Merkle†
Purdue University, West Lafayette, Indiana 47907
W. M. Scott‡
Aerospace Testing Alliance, Inc., Arnold Air Force Base, Tennessee 37389
and
D. Keefer,§ T. Moeller,¶ and R. Rhodes**
University of Tennessee Space Institute, Tullahoma, Tennessee 37388

DOI: 10.2514/1.J050353

A numerical procedure that applies to both the magnetic diffusion and wave propagation regimes of a general plasma/electromagnetic system is presented. The method solves the full Maxwell equations, with or without displacement current, in combination with the Navier–Stokes equations. The combined system is placed in a fully coupled conservation form and embedded in a dual-time formulation that enables classical hyperbolic solution algorithms to be effective across the wave and diffusion limits of the Maxwell equations. The dual-time formulation introduces a pseudotime with an artificial speed of light that includes divergence constraints that are driven to zero by means of a Lagrange multiplier technique. The validity of the algorithm is first established by verifying results obtained with the hyperbolic procedure for the diffusion form of the telegraph equation against analytical solutions. Additional verification for the electromagnetic equations is obtained by comparison with magnetic diffusion simulations obtained from the MACH2 code. Representative numerical calculations are presented for both the wave and magnetic diffusion limits to illustrate the importance of a solution technique that handles all regimes, from insulators to conductors.

Nomenclature

$\mathbf{B}$	=	magnetic induction
c	=	speed of light
$\mathbf{E}$	=	electric field
e	=	electron charge
J	=	current density
L	=	characteristic length scale
n	=	electron number density
S^{em}	=	Poynting vector
t	=	physical time
u^{em}	=	electromagnetic energy
β	=	pseudotime scaling coefficient
ε_0	=	electric permittivity
μ_0	=	magnetic permeability
ρ_e	=	electric charge density
σ	=	electrical conductivity
τ	=	pseudotime
τ^{em}	=	electromagnetic shear stress tensor
τ^{vis}	=	viscosity shear stress tensor
φ_B	=	Lagrange multiplier for divergence constraint on B field
φ_E	=	Lagrange multiplier for divergence constraint on E field

Subscript

r	=	reference quantity

Superscripts

n	=	physical time step
k	=	pseudotime step
*	=	dimensionless variable

Presented as Paper 2007-5745 at the 43rd AIAA/ASME/SAE/ASEE Joint Propulsion Conference and Exhibit, Cincinnati, OH, 8–11 July 2007; received 20 November 2009; revision received 6 May 2010; accepted for publication 14 May 2010.

*Research Assistant Professor, Mechanical Engineering; dli@purdue.edu.
†Reilly Professor of Engineering, Aerospace Engineering; merkle@ecn.purdue.edu.
‡Senior Engineer, Space and Missiles Projects, Mail Stop 6700; W.Michael.Scott@arnold.af.mil.
§Professor Emeritus, Engineering Science, Center for Laser Applications; d_keefer@bellsouth.net.
¶Assistant Professor, Aerospace and Mechanical Engineering; tmoeller@utsi.edu.
**Research Scientist, Center for Laser Applications; brhodes@utsi.edu.

I. Introduction

IN MANY engineering applications involving plasmas, the magnetic diffusion (MHD) approximation to Maxwell's equations is used to provide a simplified equation system that is coupled with the equations of fluid mechanics [1–3]. The MHD approximation involves three basic postulates: first, that the displacement current, $(1/c^2)\partial\mathbf{E}/\partial t$, can be neglected in comparison with the conduction current; second, that the current flow due to charge transport can be neglected in comparison with the conduction current; and third, that the electrostatic body force term in the fluid dynamic momentum equation can be neglected in comparison with the magnetic body force term. This approximation clearly depends upon the time rate of change of the electric field and, in many applications, the electric permittivity is small enough that it is easily valid (examples being MHD generators [4] and accelerators or high-power arc heaters [5]), but in fast transient problems such as those involved in high-power plasma switches [6,7] and pulsed plasma thrusters [8], there are often localized regions in the flowfield where this approximation is violated, and predictions from the MHD approximation are a poor approximation of the physics. All MHD codes suffer from an inability to accurately model the electromagnetic equations in regions where dense plasma transitions to

vacuum. Various numerical techniques have been employed in these codes to overcome this serious deficiency in the MHD approximation [9]. This problem often arises in the early time modeling of fast pulse devices, such as opening switches and pulsed plasma thrusters. The vacuum region, where wave propagation of the magnetic field dominates, is often modeled by the injection of field-carrying fluid into the vacuum region or filling the region with etherlike fluids with no mass and a finite electrical diffusivity to simulate the propagation of electromagnetic fields through a vacuum. However, these approaches do not properly model the physics, and they require the use of arbitrary parameters chosen to comply with observed behavior [10]. Methods for accurately treating such regions where the MHD approximation is not valid require the use of the full Maxwell equations in conjunction with the equations of fluid dynamics.

Mathematically, dropping the temporal derivative corresponding to the displacement current constitutes a singular perturbation problem in which the character of the equations is changed from hyperbolic to parabolic. For example, it is well known that the propagation of electromagnetic fields in free space occurs by means of wave processes. The corresponding mathematical character of Maxwell's equations in a vacuum is, therefore, hyperbolic. By contrast, when electromagnetic fields travel through a medium with finite conductivity, a source term appears in the equations and alters their eigenvalues. For sufficiently large values of the conductivity, this source term changes the character of the equations from hyperbolic to parabolic, a change that is directly indicative of the singular perturbation nature of the MHD approximation. Specifically, the MHD equations correspond to this diffusive limit of Maxwell's equations and describe the propagation of magnetic fields by diffusion.

In the present paper, we develop a computational algorithm that enables the coupled system composed of the Navier–Stokes equations and either the full Maxwell equations or their MHD approximations to be solved numerically by a single hyperbolic procedure. The development starts by expressing the combined Maxwell/Navier–Stokes system as a coupled first-order system in strong conservation form. The common numerical procedure is then enabled by adding pseudotime derivatives to all equations in the system. The coefficients of the pseudotime terms are selected so that the system remains hyperbolic in pseudotime, independent of the character of the equation system in physical time. This pseudotime is then used as the basis for a dual-time computational algorithm that employs standard hyperbolic procedures of contemporary numerical techniques. The addition of a pseudotime to the divergence constraints enables them to be driven to zero by means of a Lagrange multiplier technique.

Following the numerical development, we present some verification of our computer code, GEMS, by comparing its results with those from analytical solutions and a widely accepted MHD code (MACH2). Some representative solutions of physical problems in which magnetic fields are propagated by both wave and diffusion mechanisms in different parts of the computational domain are then presented. We close with some representative results obtained with the hyperbolic method for a problem for which the MHD approximation is acceptable throughout to demonstrate that the method remains efficient and accurate in the MHD limit as well.

The organization of the paper is a follows. Section II discusses the development of the equation system and the coupling between the fluid and electromagnetic systems. Section III discusses the implementation of the hyperbolic algorithm that is applicable to either the MHD equations or the complete Maxwell set. Section IV then presents verification of our computer code on some simple test problems against closed-form analytical solutions and corresponding MACH2 calculations. Section V summarizes our findings.

II. Coupled Fluids/Plasma/Maxwell Equations

In the present section, we present the equations for electromagnetic fields and fluid mechanics and express them as a coupled first-order system in strong conservation form. The formulation of the electromagnetic equations retains all terms in the full Maxwell equations without invoking the MHD approximation, therefore making them applicable in either the wave or diffusion propagation limits. The fluid formulation comprises the complete Navier–Stokes equations along with a model equation for the effects of turbulence. The partial differential equations of the general electromagnetic/fluids system are closed by appropriate constitutive relations. A generalized Ohm's law that includes a Hall current is used to close the electromagnetic equations, and an arbitrary equation of state expressed in terms of the Gibbs function is used for the fluids. It is noteworthy that the coupled formulation handles the Hall term as an integral part of the formulation, not as an add-on effect.

A. Maxwell's Equations

Maxwell's equations describe the propagation of electromagnetic energy through various types of media. In their most general form, these equations can be written as

$$\nabla \cdot \mathbf{B} = 0, \qquad \nabla \times \mathbf{E} + \frac{\partial \mathbf{B}}{\partial t} = 0$$
$$\nabla \cdot \mathbf{D} = \rho_e, \qquad \nabla \times \mathbf{H} - \frac{\partial \mathbf{D}}{\partial t} = \mathbf{J} \tag{1}$$

where $\mathbf{E}$ is the electric field, $\mathbf{D}$ is the electric displacement vector, $\mathbf{B}$ is the magnetic induction vector (magnetic flux density), $\mathbf{H}$ is the magnetic field intensity, $\mathbf{J}$ is the current density, and ρ_e is the electric charge density. The constitutive relations between $\mathbf{E}$ and $\mathbf{D}$, and $\mathbf{B}$ and $\mathbf{H}$, for free space are given by $\mathbf{D} = \varepsilon_0 \mathbf{E}$ and $\mathbf{H} = \mathbf{B}/\mu_0$, where $\varepsilon_0 = 8.854187817 \times 10^{-12}$ F/m and $\mu_0 = 4\pi 10^{-7}$ N/A^2 are the electric permittivity and the magnetic permeability of free space, respectively. The inverse of the square root of their product defines the speed of light in vacuum:

$$c = 1/\sqrt{\varepsilon_0 \mu_0} = 2.99792458 \times 10^8 \text{ m/s}$$

In a more general form, $\mathbf{H}$ and $\mathbf{D}$ are not unique functions of $\mathbf{B}$ and $\mathbf{E}$, but they depend upon their earlier time evolution and are given by $\mathbf{D} = \varepsilon_0 \mathbf{E} + \mathbf{P}$ and $\mathbf{H} = \mathbf{B}/\mu_0 - \mathbf{M}$, where $\mathbf{P}$ is the polarization vector and $\mathbf{M}$ is the magnetization vector. For the fluid media of interest here, the simpler relations apply.

With the simplification of a linear, isotropic medium, Maxwell's equations become

Faraday's law,

$$\frac{\partial \mathbf{B}}{\partial t} + \nabla \times \mathbf{E} = 0 \tag{2}$$

Gauss' law (divergence constraint on electric field),

$$\nabla \cdot \mathbf{E} = \rho_e / \varepsilon_0 \tag{3}$$

the divergence constraint on the magnetic field,

$$\nabla \cdot \mathbf{B} = 0 \tag{4}$$

and Ampere's law,

$$\frac{1}{c^2} \frac{\partial \mathbf{E}}{\partial t} - \nabla \times \mathbf{B} = -\mu_0 \mathbf{J} \tag{5}$$

Closure of this set of partial differential equations requires an additional auxiliary relation to express the electrical current as a function of the electromagnetic fields and the properties of the medium with which they are coupled. For applications in which electron/ion collision times are small compared with the time scale of interest, the plasma can be approximated as being in thermal equilibrium, and the plasma can be well represented by a single, ohmic fluid. The current may then be written in terms of convective and conductive contributions:

$$\mathbf{J} = \rho_e \mathbf{v} + \mathbf{J}_c \tag{6}$$

where $\mathbf{v}$ is the plasma velocity and J_c is the conductive current. Including the Hall effect, the conduction current, the plasma velocity,

the electron number density n, and the electrical conductivity σ are related to the electromagnetic fields by the generalized Ohm's law:

$$\mathbf{E} = -\mathbf{v} \times \mathbf{B} + \frac{1}{\sigma}\mathbf{J}_c + \frac{1}{ne}\mathbf{J}_c \times \mathbf{B} \tag{7}$$

Ohm's law represents an approximate empirical expression but is sufficient to close the Maxwell system. For convenience, it can be inverted to express the current density in terms of the electric and magnetic fields by defining a general electrical conductivity tensor $\mathbf{\Lambda}$ as

$$\mathbf{\Lambda}^{-1} = \frac{1}{\sigma}\begin{bmatrix} 1 & 0 & 0 \\ 0 & 1 & 0 \\ 0 & 0 & 1 \end{bmatrix} + \frac{1}{ne}\begin{bmatrix} 0 & -B_z & B_y \\ B_z & 0 & -B_x \\ -B_y & B_x & 0 \end{bmatrix}$$
$$= \frac{1}{\sigma}\begin{bmatrix} 1 & -B_z\sigma/ne & B_y\sigma/ne \\ B_z\sigma/ne & 1 & -B_x\sigma/ne \\ -B_y\sigma/ne & B_x\sigma/ne & 1 \end{bmatrix} \tag{8}$$

to give

$$\mathbf{J}_c = \mathbf{\Lambda}(\mathbf{E} + \mathbf{v} \times \mathbf{B}) \tag{9}$$

Note that the matrix $\mathbf{\Lambda}$ is a function of the magnetic field, as noted in the last expression in Eq. (8). In the limit, when the plasma velocity is zero, Eq. (9) defines an effective electrical conductivity as a tensor quantity. For a solid, Ohm's law reduces to the simple form, $\mathbf{J}_c = \sigma\mathbf{E}$.

The electrical conductivity and the number density of electrons likewise require constitutive relations. For the present analysis, we express these as general thermodynamic functions of the pressure and temperature in the material: $\sigma = \sigma(p, T)$ and $n = n(p, T)$. As shown later, this (p, T) dependence is consistent with the primary dependent variables chosen for the fluid dynamics and facilitates the coupled solution procedure. The conductivity is clearly a material property and can be represented in terms of thermodynamic variables only, but expressing the electron number density as a function of p and T requires thermodynamic equilibrium. For cases where this approximation is not appropriate, the electron number density can be obtained from a chemical kinetic/Saha rate expression and multiple species conservation equations. Using rate processes to compute the electron number density (in principle) does not impact the solution procedure presented here (apart from increasing the number of equations). Thus, without loss of generality, the simpler algebraic system based on thermodynamic equilibrium is chosen here to present the solution procedure.

B. Wave Propagation and Diffusion in Maxwell's Equations

Maxwell's equations in a vacuum or an ideal insulator represent a hyperbolic system in which disturbances propagate as waves. Their character, however, changes as the conductivity of the medium increases until they eventually approximate a diffusive, as opposed to a wave, system. This diffusive limit of Maxwell's equations corresponds to the MHD approximation. Before looking at the MHD equations, to illustrate the transition between the two diverse limits of Maxwell's equations, we will combine a simplified version of them into a single equation. Because the key approximation in the MHD equations is to drop the displacement current, we modify Ampere's law by multiplying the displacement current term by the parameter κ, so that Eq. (5) becomes

$$\frac{\kappa}{c^2}\frac{\partial \mathbf{E}}{\partial t} - \nabla \times \mathbf{B} = -\mu_0\mathbf{J} \tag{10}$$

For $\kappa = 1$, we have the Maxwell equations; for $\kappa = 0$, we have the MHD approximation. To simplify the algebra, we ignore Hall currents and fluid velocity, simplify Ohms's law to the scalar form, $\mathbf{J} = \sigma\mathbf{E}$, and take the electrical conductivity as a constant.

These simplifications allow us to eliminate the current density from the modified Ampere's law in Eq. (10) and, upon combining it with Faraday's law [Eq. (2)], to eliminate the electric field $\mathbf{E}$. This gives an equation for the magnetic field only:

$$\frac{\kappa}{c^2}\frac{\partial^2 \mathbf{B}}{\partial t^2} + \mu_0\sigma\frac{\partial \mathbf{B}}{\partial t} = \nabla^2\mathbf{B} \tag{11}$$

The combination of first- and second-order temporal derivatives on the left-hand side of Eq. (11) indicates that the fundamental mathematical character of the equation is governed by the relative magnitudes of the two temporal derivatives. These, in turn, are determined by the values of the parameter κ and the electrical conductivity σ. When $\kappa = 1$ (the Maxwell equations with the displacement current retained) and $\sigma = 0$ (an ideal insulator), the first-derivative term vanishes, and Eq. (11) becomes the classical second-order hyperbolic wave equation:

$$\frac{\kappa}{c^2}\frac{\partial^2 \mathbf{B}}{\partial t^2} = \nabla^2\mathbf{B} \tag{12}$$

and magnetic fields are propagated by wave processes. When the parameter $\kappa = 0$ (the MHD equations with the displacement current dropped) and $\sigma \neq 0$ (a real insulator or conductor), the equation reduces to the parabolic equation:

$$\frac{\partial \mathbf{B}}{\partial t} = \frac{1}{\mu_0\sigma}\nabla^2\mathbf{B} \tag{13}$$

and magnetic fields are propagated by diffusive processes. This represents the MHD limit. This simple example shows that dropping the displacement current represents a singular perturbation in that the order of the temporal derivatives in the equation system is reduced by one.

Clearly, the MHD equations are contained within the complete Maxwell equation, and this same change of character is observed when the parameter κ is set to unity and the value of the electrical conductivity σ is varied. When the electrical conductivity is small but finite, the equation is hyperbolic, and the solutions are wavelike in nature. As the electrical conductivity is increased, the source term in Ampere's law [the first-derivative term in Eq. (11)] alters the mathematical character of the equation in continuous fashion until its eigenvalues become complex and its solutions become diffusive in nature.

Similar conclusions concerning the change of character in Maxwell's equations can be reached when the complete Ohm's law with variable electrical conductivity, the $\mathbf{v} \times \mathbf{B}$ term, and the Hall term are retained. As the displacement current gets smaller (the first-order time derivative becomes more significant than the second-order time derivative), the character of the equation changes to a diffusion equation. Thus, while dropping the displacement current changes the character of the equation system in a discontinuous fashion, retaining the displacement current, while increasing the conductivity, changes the character of the equation in a continuous fashion. This continuous transition from wavelike to diffusionlike constitutes the basis upon which systems containing both wave and diffusive limits in the same problem can be solved by a single numerical algorithm.

This simple derivation demonstrates the important concept that, when the conductivity of the material of interest is zero (or small), electromagnetic energy travels as a wave, and the equations correspond to a hyperbolic system. In a vacuum, these waves propagate at the speed of light. In the limit of very good conductors, the second-order time derivative can be neglected, and the equation degenerates to a diffusion operator. Thus, in very good conductors, the eigenvalues of the system revert from a pair of real eigenvalues to an imaginary pair, and the magnetic field diffuses through the material. This important distinction between Maxwell's equations and the MHD approximation has a major impact in the types of numerical methods that are used to solve the two systems. The present paper outlines a common method that uses hyperbolic marching in a pseudotime rather than physical time to solve either the Maxwell equations or the MHD approximation. We now present a more formal representation of the MHD approximation.

C. Magnetic Diffusion Equations

In the limit, when the displacement current may be neglected, Maxwell's equations can be combined to give the MHD equation. Formally, this is done by dropping the displacement current in Ampere's law and combining it with Faraday's law and the complete form of Ohm's law to give

$$\frac{\partial \mathbf{B}}{\partial t} - \nabla \times (\mathbf{v} \times \mathbf{B}) + \nabla \times \left(\frac{\nabla \times \mathbf{B}}{\mu_0 \sigma} \right) + \nabla \times \left\{ \frac{1}{\mu_0 n e} (\nabla \times \mathbf{B}) \times \mathbf{B} \right\} = 0 \tag{14}$$

The mathematical operations needed for obtaining Eq. (14) are slightly different than those used to obtain the combined relation (13), but the steps are quite straightforward. The important fact is that electric field has been eliminated to obtain an uncoupled diffusion equation for the magnetic field. In particular, the second term in Eq. (14) is a convective term that represents the convection of the magnetic field by the plasma, while the remaining two second-derivative terms represent diffusion of the magnetic field. Consequently, dropping the displacement current again changes the characteristic physics from wavelike to diffusive.

In regions where there is no electric current and no fluid velocity, the magnetic induction equation reduces to the statement that the magnetic field $\mathbf{B}$ is stationary, or $\partial \mathbf{B}/\partial t = 0$. Therefore, when current is absent, magnetic fields cannot diffuse and, in the absence of velocity, they cannot convect. This represents a contradiction in transient plasma problems where the Maxwell equations will allow the wave propagation of the magnetic field in free space, but the MHD equations (more specifically, the magnetic induction equation) preclude it. The emphasis of the work described here is the formulation of a numerical algorithm that bypasses this restriction and allows wave propagation in vacuum regions without impairing the computational efficiency in regions where the MHD approximations remain valid. In particular, an algorithm that applies equally to Maxwell's equations and the magnetic induction equation is proposed next.

For numerical solution purposes, it is pertinent to note that the magnetic induction equation requires less storage than do solutions of the full Maxwell equations, since only one vector field must be stored in the MHD system as compared with two in the full equations. While this was a very important consideration several years ago when computer memory was much more expensive, present memory costs are such that this difference is no longer significant. The disadvantage of the MHD system is that, once the magnetic field is obtained, the electric field must be obtained by differentiation of the magnetic field, resulting in increased errors. By contrast, the method described in the present paper solves for (and therefore must store) both the E and B fields, but the electric field is computed directly from its own equation without differentiation. Finally, we note that, although the MHD equation requires the solution of only one equation while the present method requires the solution of two, the operation count for the two methods is nearly the same, because the MHD equation is second order while the E-B system is composed of two first-order equations.

D. Fluid Dynamic Conservation Equations

The formulation of a comprehensive three-dimensional viscous plasma model requires that the conservation laws of fluid dynamics be combined with the complete Maxwell equations. The equation set for the fluid dynamic portion of the problem is given by

the conservation of mass,

$$\frac{\partial \rho}{\partial t} + \nabla \cdot (\rho \mathbf{v}) = 0 \tag{15}$$

the conservation of momentum,

$$\frac{\partial \rho \mathbf{v}}{\partial t} + \nabla \cdot (\rho \mathbf{v}\mathbf{v} + p\mathbf{I}) = \nabla \cdot \boldsymbol{\tau} + \mathbf{J} \times \mathbf{B} + \boldsymbol{\rho}_e \mathbf{E} e \tag{16}$$

and the conservation of energy,

$$\frac{\partial (\rho h_0 - p)}{\partial t} + \nabla \cdot (\rho h_0 \mathbf{v}) = -\nabla \cdot \mathbf{q} + \nabla \cdot (\boldsymbol{\tau} \cdot \mathbf{v}) + \mathbf{J} \cdot \mathbf{E} \tag{17}$$

where $\mathbf{J} \times \mathbf{B} + \rho_e \mathbf{E}$ and $\mathbf{J} \cdot \mathbf{E}$ are source terms representing the Lorentz force and the electrical power dissipation, respectively. These two source terms can, however, be converted into conservation form by expressing them in terms of an appropriate set of primary variables. The $\mathbf{J} \cdot \mathbf{E}$ term in the energy equation is considered first, followed by the $\mathbf{J} \times \mathbf{B} + \rho_e \mathbf{E}$ term.

Using Ampere's law to replace the current density in the $\mathbf{J} \cdot \mathbf{E}$ expression gives

$$\mathbf{J} \cdot \mathbf{E} = \mathbf{E} \cdot \mathbf{J} = \frac{1}{\mu_0} \mathbf{E} \cdot \left(-\frac{1}{c^2} \frac{\partial \mathbf{E}}{\partial t} + \nabla \times \mathbf{B} \right) \tag{18}$$

Next, the vector identity,

$$\nabla \cdot (\mathbf{E} \times \mathbf{B}) \equiv \mathbf{B} \cdot \nabla \times \mathbf{E} - \mathbf{E} \cdot \nabla \times \mathbf{B}$$

is introduced to obtain

$$\mathbf{J} \cdot \mathbf{E} = \frac{1}{\mu_0} \left\{ -\frac{1}{c^2} \frac{\partial \mathbf{E}}{\partial t} \cdot \mathbf{E} + \mathbf{B} \cdot (\nabla \times \mathbf{E}) - \nabla \cdot (\mathbf{E} \times \mathbf{B}) \right\} \tag{19}$$

Faraday's law can then be used to replace the $\nabla \times \mathbf{E}$ term, giving

$$\mathbf{J} \cdot \mathbf{E} = -\frac{1}{\mu_0} \left\{ \frac{1}{c^2} \frac{\partial \mathbf{E}}{\partial t} \cdot \mathbf{E} + \frac{\partial \mathbf{B}}{\partial t} \cdot \mathbf{B} + \nabla \cdot (\mathbf{E} \times \mathbf{B}) \right\} \tag{20}$$

Finally, defining the Poynting vector, $\mathbf{S}^{\text{em}} = (\mathbf{E} \times \mathbf{B})/\mu_0$, and the electromagnetic energy density, $u^{\text{em}} = (1/2\mu_0)\{(\mathbf{E} \cdot \mathbf{E})/c^2 + \mathbf{B} \cdot \mathbf{B}\}$, yields the conservative form:

$$\mathbf{J} \cdot \mathbf{E} = -\frac{\partial u^{\text{em}}}{\partial t} - \nabla \cdot \mathbf{S}^{\text{em}} \tag{21}$$

A similar manipulation casts the electromagnetic force density in the momentum equation into conservation form. Starting from the momentum source term and using Ampere's law to eliminate the current density and Gauss's law to eliminate the charge density gives

$$\mathbf{J} \times \mathbf{B} + \rho_e \mathbf{E} = \frac{1}{\mu_0} \left(-\frac{1}{c^2} \frac{\partial \mathbf{E}}{\partial t} + \nabla \times \mathbf{B} \right) \times \mathbf{B} + \varepsilon_0 \mathbf{E} (\nabla \cdot \mathbf{E}) \tag{22}$$

Expanding the unsteady term and adding the divergence of the magnetic field (which is zero) gives

$$\mathbf{J} \times \mathbf{B} + \rho_e \mathbf{E} = \frac{1}{\mu_0} \left[-\frac{1}{c^2} \frac{\partial (\mathbf{E} \times \mathbf{B})}{\partial t} + \frac{1}{c^2} \mathbf{E} \times \frac{\partial \mathbf{B}}{\partial t} - \mathbf{B} \times \nabla \times \mathbf{B} + \mathbf{B} (\nabla \cdot \mathbf{B}) + \frac{\mathbf{E} (\nabla \cdot \mathbf{E})}{c^2} \right] \tag{23}$$

Next, Faraday's law may be used to eliminate the time derivative of the magnetic field and obtain

$$\mathbf{J} \times \mathbf{B} + \rho_e \mathbf{E} = \frac{1}{\mu_0} \left[-\frac{1}{c^2} \frac{\partial (\mathbf{E} \times \mathbf{B})}{\partial t} + \frac{\mathbf{E} (\nabla \cdot \mathbf{E}) - \mathbf{E} \times \nabla \times \mathbf{E}}{c^2} + \mathbf{B} (\nabla \cdot \mathbf{B}) - \mathbf{B} \times \nabla \times \mathbf{B} \right] \tag{24}$$

Finally, combining the previous definition of the Poynting vector along with a new definition for the electromagnetic shear stress,

$$\nabla \cdot \boldsymbol{\tau}^{\text{em}} = \frac{1}{\mu_0} \nabla \cdot \left(\frac{\mathbf{E}\mathbf{E}}{c^2} + \mathbf{B}\mathbf{B} \right) - \nabla \left(\frac{\mathbf{E} \cdot \mathbf{E}}{c^2} + \mathbf{B} \cdot \mathbf{B} \right) \tag{25}$$

the conservative form for the Lorentz force is obtained:

$$\mathbf{J} \times \mathbf{B} + \rho_e \mathbf{E} = -\frac{1}{c^2}\frac{\partial \mathbf{S}^{\mathrm{em}}}{\partial t} + \nabla \cdot \boldsymbol{\tau}^{\mathrm{em}} \tag{26}$$

Note that the scalar form of the electromagnetic shear stress term is

$$\tau_{\alpha\beta}^{\mathrm{em}} = \frac{1}{\mu_0}\left(\frac{\mathbf{E}_\alpha \mathbf{E}_\beta}{\mathbf{c^2}} + \mathbf{B}_\alpha \mathbf{B}_\beta\right) - \delta_{\alpha\beta}\mathbf{u}^{em} \tag{27}$$

Using the conservation relations in Eqs. (21) and (27), the source terms in the energy and momentum equations may then be absorbed into the convection and time derivative terms of the fluid equations, resulting in the strongly conservative system:

$$\frac{\partial \rho}{\partial t} + \nabla \cdot \rho \mathbf{v} = 0 \tag{28}$$

$$\frac{\partial}{\partial t}\left(\rho \mathbf{v} + \frac{\mathbf{S}^{\mathrm{em}}}{c^2}\right) + \nabla \cdot (\rho \mathbf{v}\mathbf{v} - \boldsymbol{\tau}^{\mathrm{em}}) + \nabla p = \nabla \cdot \boldsymbol{\tau}^{\mathrm{vis}} \tag{29}$$

$$\frac{\partial}{\partial t}(\rho h^0 - p + u^{\mathrm{em}}) + \nabla \cdot (\rho \mathbf{v} h^0 + \mathbf{S}^{\mathrm{em}}) = \nabla \cdot (\boldsymbol{\tau}^{\mathrm{vis}} \cdot \mathbf{v} + k\nabla T) \tag{30}$$

In this form, all sources have been removed from the fluids equations.

E. Constitutive Relations for Fluids and System Closure

The conservation laws of fluid dynamics [Eqs. (28–30)] and electromagnetics [Eqs. (2–6)] form a mutually coupled system of partial differential equations, but a count of equations and unknowns indicates that system closure requires additional equations. To this end, a generalized Ohm's law [Eq. (8)] has already been introduced in the Maxwell section. A similar set of constitutive relations is needed for the thermodynamic and transport properties of the working fluid. The thermodynamic properties of the fluid can be described by defining the Gibbs free energy as an arbitrary function of pressure and temperature:

$$g = g(p, T) \tag{31}$$

Once the Gibbs function is defined, the density, entropy, and enthalpy of the fluid are then readily obtained from its partial derivatives:

$$\rho(p, T) = \frac{1}{g_p}, \qquad s(p, T) = -g_T \tag{32}$$

and

$$h(p, T) = g - T g_T$$

where subscripts imply partial differentiation with the alternative variable held constant. For completeness, four additional partial derivatives that are used later are also defined:

$$\rho_p = -\frac{g_{pp}}{g_p^2}, \qquad \rho_T = -\frac{g_{pT}}{g_p^2}, \qquad h_p = g_p - T g_{pT} \tag{33}$$

and

$$h_T = g_{TT}$$

Note that the last quantity is the specific heat at constant pressure. The manner in which these four property derivatives enter the computational formulation is given next. By starting from a common Gibbs free energy, it is assured that the property set is thermodynamically consistent. As two final terms, we introduce the stagnation enthalpy h^0 and the speed of sound c_f in a general fluid:

$$h^0 \equiv h + \rho \bar{\mathbf{v}} \cdot \bar{\mathbf{v}} \tag{34}$$

and

$$c_f^2 = \left(\frac{\partial p}{\partial \rho}\right)_s = \frac{\rho h_T}{\rho \rho_p h_T + \rho_T (1 - \rho h_p)}$$

In addition to thermodynamic properties, it is also necessary to specify transport properties. For consistency with the primitive variables form of the Gibbs function (and the primitive variables form of the numerical solution method given next), the viscosity, thermal conductivity, and electrical conductivity are also specified as arbitrary functions of pressure and temperature:

$$\mu = \mu(p, T), \qquad k = k(p, T) \tag{35}$$

and

$$\sigma = \sigma(p, T)$$

Note that the Gibbs function in Eq. (33) and the transport properties in Eq. (35) can be specified as algebraic or tabular functions from the best available source for the selected working fluid.

For computations of a general nature, it is also necessary to incorporate a turbulence model of an algebraic, single, or multiple equation format. Since the turbulence model has little effect on the numerical algorithm, the details are not included.

III. Numerical Implementation

The conservation laws for fluids [Eqs. (28–30)] and electromagnetic effects [Eqs. (2–6)], along with Ohm's law [Eq. (8)], the thermodynamic constitutive relations and transport properties [Eqs. (31–35)], and an appropriate turbulence model (not given here) form the complete equation set for modeling an arbitrary fluids/electromagnetic interaction. This equation system is highly nonlinear and, as with the conservation laws from nearly all branches of physics, its numerical discretization generates wide-banded matrices that are expensive to invert. Both the nonlinearity and the wide-banded matrices dictate the use of iterative solution methods. The advantage of the present system over traditional couplings between the MHD equation and the fluids equations is that, now, both sets of equations (electromagnetic and fluids) are of similar first-order form. This immediately suggests the use of classical hyperbolic time-marching procedures, but there are several drawbacks. First, simply retaining the displacement current in regions in which it is small will lead to numerical difficulties for two reasons. When the term is small, the equations will be stiff, and time-marching methods will become excruciatingly slow. Even with this term included, the current density term in Ampere's law renders the system parabolic, so a hyperbolic procedure becomes problematic even if it is slow.

A second shortcoming is the appearance of the divergence constraints in Maxwell's equations. From an analytical perspective, if the divergence constraints are satisfied initially, and Ampere's and Faraday's laws are solved exactly, the divergence constraints remain satisfied for all time. Numerical solutions, however, are subject to growing computational errors that manifest themselves as violations of the divergence constraints and, eventually, completely dominate the solutions. Some method must be developed for enforcing these constraints. Both of these primary difficulties can be handled by simple methods that have long been implemented in computational fluid dynamics solutions. For example, the restriction from compressible to incompressible flows introduces a similar singular perturbation into fluid dynamics problems. This singularity is routinely circumvented by adding a pseudotime derivative to the continuity equation. The equations then become hyperbolic in pseudotime with an artificial speed of sound for which the magnitude can be controlled to be of the same order as the velocity for all conditions by appropriate scaling of the pseudotime derivative. An identical method can be used in the Maxwell equations. Introducing a pseudotime with an artificial speed of light provides a hyperbolic system that remains well conditioned in all limits. Finally, the introduction of a pseudotime with the divergence constraints enables

them to be driven to zero by means of a Lagrange multiplier technique [11].

The addition of a pseudotime derivative to the space-time conservation relations provides a physically based iteration path that is applicable to both steady and transient calculations. For steady-state solutions, pseudotime provides an evolution from some arbitrary initial condition to a converged steady result (assuming one exists). For time-accurate calculations, pseudotime allows iterations at each physical time step to improve the accuracy of the transient solution while also enabling larger physical time steps. The present pseudotime formulation ensures that the system remains hyperbolic with a complete independent variables vector, even in cases where the final solutions are parabolic in physical time. This implies that a single computational technique can be used for both the Maxwell and the MHD limits of the coupled fluids/electromagnetic problem.

To implement the hyperbolic, pseudotime procedure in the present system, we add a pseudotime derivative to all equations in the system, including the divergence constraints. With the Lagrange multiplier divergence constraints included, the system swells to 11 equations. Denoting the physical time by t and the pseudotime by τ, the modified equations become

$$\frac{\partial \mathbf{B}}{\partial \tau} + \frac{\partial \mathbf{B}}{\partial t} + \nabla \times \mathbf{E} + \nabla \phi_E = 0 \tag{36}$$

$$\frac{1}{\beta^2 c^2}\frac{\partial \mathbf{E}}{\partial \tau} + \frac{1}{c^2}\frac{\partial \mathbf{E}}{\partial t} - \nabla \times \mathbf{B} + \nabla \phi_B = -\mu_0(\rho_e \mathbf{v} + \mathbf{J}_c) \tag{37}$$

$$\frac{1}{\beta^2 c^2}\frac{\partial \phi_B}{\partial \tau} + \nabla \cdot \mathbf{B} = 0 \tag{38}$$

$$\frac{\partial \phi_E}{\partial \tau} + \frac{1}{\sigma}\nabla \cdot \mathbf{J} = \rho_e/\varepsilon_0 \tag{39}$$

$$\frac{\partial \rho}{\partial \tau} + \frac{\partial \rho}{\partial t} + \nabla \cdot \rho \mathbf{v} = 0 \tag{40}$$

$$\frac{\partial}{\partial \tau}\left(\rho \mathbf{v} + \frac{\mathbf{S}^{\mathrm{em}}}{c^2}\right) + \frac{\partial}{\partial t}\left(\rho \mathbf{v} + \frac{\mathbf{S}^{\mathrm{em}}}{c^2}\right) + \nabla \cdot (\rho \mathbf{v}\mathbf{v} - \boldsymbol{\tau}^{\mathrm{em}}) + \nabla p = \nabla \cdot \boldsymbol{\tau}^{\mathrm{vis}} \tag{41}$$

$$\frac{\partial}{\partial \tau}(\rho h^0 - p + u^{\mathrm{em}}) + \frac{\partial}{\partial t}(\rho h^0 - p + u^{\mathrm{em}}) + \nabla \cdot (\rho \mathbf{v} h^0 + \mathbf{S}^{\mathrm{em}}) = \nabla \cdot (\boldsymbol{\tau}^{\mathrm{vis}} \cdot \mathbf{v} + k \nabla T) \tag{42}$$

Dimensional consistency has been ensured in the pseudotime terms by using the same quantities as in the physical time derivatives, except for multiplying selected terms by the dimensionless scaling parameter β. To preclude difficulties with the divergence constraint on the electric field, we have replaced it by enforcing the current density to be divergenceless. This approximation is rigorous for steady problems, except at material interfaces where there is a step change in conductivity that is calculable and can be added to the constraint. In unsteady problems, it appears to work effectively, but it requires additional study.

Note that the pseudotime terms are added to the full unsteady equations so that either steady or transient solutions can be computed. For steady solutions, the physical time derivatives are omitted, and the solution evolution is followed in pseudotime in the traditional time-marching manner. For unsteady solutions, the physical time is retained, and the solution at each physical time step is marched in pseudotime until such time that all linearization and factorization errors have been removed, as outlined next.

To facilitate understanding, the pseudotime form of the coupled fluids/electromagnetic equations is expressed in the compact vector form:

$$\frac{\partial \mathbf{Q}'}{\partial \tau} + \frac{\partial \mathbf{Q}}{\partial t} + \nabla \cdot (\mathbf{F} - \mathbf{F}_v) = \mathbf{H} \tag{43}$$

where

$$Q' = \begin{pmatrix} \rho \\ \rho \mathbf{v} + \mathbf{S}^{\mathrm{em}}/c^2 \\ h^0 - p + u^{\mathrm{em}} \\ \mathbf{B} \\ \mathbf{E}/\beta^2 c^2 \\ \phi_B/\beta^2 c^2 \\ \sigma \phi_e \end{pmatrix}, \qquad Q = \begin{pmatrix} \rho \\ \rho \mathbf{v} + \mathbf{S}^{\mathrm{em}}/c^2 \\ \rho h^0 - p + u^{\mathrm{em}} \\ \mathbf{B} \\ \mathbf{E}/c^2 \\ 0 \\ 0 \end{pmatrix}$$

$$\mathbf{F} = \begin{pmatrix} \rho \mathbf{v} \\ \rho \mathbf{v}\mathbf{v} - \boldsymbol{\tau}^{\mathrm{em}} + \mathbf{I}_{\mathbf{p}} \\ \rho \mathbf{v} h^0 + \mathbf{S}^{\mathrm{em}} \\ \mathbf{I} \times \mathbf{E} + \mathbf{I}\phi_E \\ -\mathbf{I} \times \mathbf{B} + \mathbf{I}\phi_B \\ \mathbf{B} \\ \mathbf{J} \end{pmatrix}, \qquad \mathbf{F}_v = \begin{pmatrix} 0 \\ \boldsymbol{\tau}^{\mathrm{vis}} \\ \boldsymbol{\tau}^{\mathrm{vis}} \cdot \mathbf{v} + k \nabla T \\ 0 \\ 0 \\ 0 \\ 0 \end{pmatrix}$$

$$\mathbf{H} = \begin{pmatrix} 0 \\ 0 \\ 0 \\ 0 \\ -\mu_0(\rho_e \mathbf{v} + \mathbf{J}_c) \\ 0 \\ \sigma \rho_e/\varepsilon_0 \end{pmatrix} \tag{44}$$

and $\mathbf{I}$ is a 3×3 unit matrix.

Since the artificial time derivative in Eq. (43) goes to zero as the solution at each physical time step is approached, there is no advantage to using conservative variables. A nonconservative vector will work just as well, especially in the plasma case that has widely different characteristic speeds, i.e., sound and light. Again using a formulation that retains dimensional consistency, the chain rule is used to transform the pseudotime derivative to the more convenient primitive variables,

$$\mathbf{Q}_p = (p, \mathbf{v}, T, \mathbf{B}, \mathbf{E}, \phi_B, \phi_E)^T$$

by means of the Jacobian:

$$\frac{\partial \mathbf{Q}'}{\partial \tau} = \frac{\partial \mathbf{Q}'}{\partial \mathbf{Q}_p}\frac{\partial \mathbf{Q}_p}{\partial \tau} \tag{45}$$

so that Eq. (43) takes the final form:

$$\boldsymbol{\Gamma}\frac{\partial \tilde{\mathbf{Q}}_p}{\partial \tau} + \frac{\tilde{\mathbf{Q}} - \mathbf{Q}^n}{\Delta t} + \nabla \cdot (\tilde{\mathbf{F}} - \tilde{\mathbf{F}}_v) = \tilde{\mathbf{H}} p \tag{46}$$

The Jacobian in Eq. (46) is given by the matrix.

$$\Gamma_p = \frac{\partial \mathbf{Q}'}{\partial \mathbf{Q_p}} = \begin{pmatrix} \rho_p & 0 & \rho_T & 0 & 0 & 0 & 0 \\ \rho_p \mathbf{v} & \rho \mathbf{I} & \rho_T \mathbf{v} & \boldsymbol{E} \times \mathbf{I}/c^2 & \mathbf{I} \times \mathbf{B}/c^2 & 0 & 0 \\ \rho_p h^0 - (1 - \rho h_p) & \rho \mathbf{v} & \rho_T h^0 + \rho h_T & \mu_0 \mathbf{B} & \varepsilon_0 \mathbf{E} & 0 & 0 \\ 0 & 0 & 0 & \mathbf{I} & 0 & 0 & 0 \\ 0 & 0 & 0 & 0 & \mathbf{I}/(\beta c)^2 & 0 & 0 \\ 0 & 0 & 0 & 0 & 0 & \mathbf{I}/(\beta c)^2 & 0 \\ 0 & 0 & 0 & 0 & 0 & 0 & 1 \end{pmatrix} \tag{47}$$

The values of the parameter, β in the artificial time derivative coefficient Γ_p are defined so as to provide well-conditioned eigenvalues in pseudotime, thereby ensuring both accuracy and improved convergence [12]. For the present computations, the value of β has been chosen as the minimum of

$$\beta = \min\left(1, \frac{1}{\mu_0 \sigma c L}\right) \tag{48}$$

The numerical solution of Eq. (46) is presented in two steps, starting with discretization in physical time and then following with discretization in pseudotime. Although all calculations included herein are computed with second-order accuracy, here we symbolically use first-order Euler implicit differencing in physical time to simplify the notation. In addition, we temporarily indicate spatial discretization by the subscript d. For the physical time, a superscript n is used to indicate the previous (known) time level, and a tilde is used to denote the new (unknown) time level such that, after discretizing in physical time, the equations become

$$\Gamma_p \frac{\partial \tilde{\mathbf{Q}}_p}{\partial \tau} + \frac{\tilde{\mathbf{Q}} - \mathbf{Q}^n}{\Delta t} \nabla_d \cdot (\tilde{\mathbf{F}} - \tilde{\mathbf{F}}_v) = \tilde{\mathbf{H}}_d \tag{49}$$

For cases in which the pseudotime eigenvalues are purely real, Eq. (49) represents a nonlinear evolution equation in pseudotime for the solution $\tilde{\mathbf{Q}}_p$ from the old time level n to the new time level, $n + 1$. Note that this evolution procedure depends only upon the character of the pseudotime term, not upon the physical time derivative. If, in addition to having real eigenvalues, the eigenvectors of the pseudotime derivative are distinct, the system is hyperbolic in τ and can be solved by classical time-marching algorithms, independent of whether the physical solution to which it evolves is hyperbolic or not. In particular, when the derivative, $\partial \tilde{\mathbf{Q}}_p / \partial \tau \to 0$, Eq. (49) approaches the exact nonlinear representation of the desired implicit discretization in physical time. It is particularly interesting to note that the presence of the discretized physical time derivative represents a sink (it is never a source) in the pseudotime formulation, and so it acts to hasten the approach to steady conditions in pseudotime. The pseudotime iteration may be expected to converge more and more rapidly as the magnitude of the physical time derivative increases.

The dual-time evolution to the final nonlinear value ensures that any truncation errors or factorization terms used in the implicit time step are evaluated nonlinearly, thereby precluding linearization or factorization errors. This nonlinear solution procedure enables larger physical time steps, especially in highly stretched regions such as boundary layers, thereby largely offsetting the costs of the iteration at each time level.

The discretization of Eq. (49) in pseudotime is now by Euler implicit differencing, using the superscripts k and $k + 1$ to give

$$\Gamma_p \frac{\tilde{\mathbf{Q}}_p^{k+1} - \tilde{\mathbf{Q}}_p^k}{\Delta \tau} + \frac{(\tilde{\mathbf{Q}}^{k+1} - \tilde{\mathbf{Q}}^k) + (\tilde{\mathbf{Q}}^k - \mathbf{Q}^n)}{\Delta t} + \nabla_d \cdot (\tilde{\mathbf{F}}^{k+1} - \tilde{\mathbf{F}}_v^{k+1}) = \tilde{\mathbf{H}}_d^{k+1} \tag{50}$$

Finally, spatial discretization is performed by integrating over a series of control volumes of finite size to obtain an integral relation of the form,

$$\oint_\Omega \left[\Gamma_p \frac{\tilde{\mathbf{Q}}_p^{k+1} - \tilde{\mathbf{Q}}_p^k}{\Delta \tau} + \frac{(\tilde{\mathbf{Q}}^{k+1} - \tilde{\mathbf{Q}}^k) + (\tilde{\mathbf{Q}}^k - \mathbf{Q}^n)}{\Delta t} + \nabla \cdot (\tilde{\mathbf{F}}^{k+1} - \tilde{\mathbf{F}}_v^{k+1}) \right] \mathbf{d}\Omega = \oint_\Omega \tilde{\mathbf{H}}^{k+1} \, \mathbf{d}\Omega \tag{51}$$

By invoking the theorems of Stokes and Gauss, the volume integrals can be written as surface integrals:

$$\left\{ \Gamma_p \frac{1}{\Delta \tau} + \frac{\partial \tilde{\mathbf{Q}}}{\partial \mathbf{Q}_p} \frac{1}{\Delta t} - \frac{\partial \tilde{\mathbf{H}}}{\partial \mathbf{Q}_p} \right\} \Delta \tilde{\mathbf{Q}}_p \Omega + \int_{\partial\Omega} \frac{\partial (\mathbf{n} \cdot \mathbf{F})}{\partial \mathbf{Q}_p} \Delta \mathbf{Q}_p \, \mathrm{d}\Sigma - \int_{\partial\Omega} \frac{\partial (\mathbf{n} \cdot \mathbf{F}_v)}{\partial \mathbf{Q}_p} \Delta \mathbf{Q}_p \, \mathbf{d}\Sigma = -\left\{ \int_{\partial\Omega} \mathbf{n} \cdot \tilde{\mathbf{F}} \, \mathbf{d}\Sigma - \int_{\partial\Omega} \mathbf{n} \cdot \tilde{\mathbf{F}}_v \, \mathbf{d}\Sigma + \left(\tilde{\mathbf{H}} + \frac{\tilde{\mathbf{Q}} - \mathbf{Q}^n}{\Delta t} \right) \Omega \right\} \tag{52}$$

The surface integrals require the specification of a numerical flux across each face of the selected control volume and indicate that the rate of change of the primitive variables in pseudotime is determined by the sum of fluxes across the several faces of each control volume. An upwind scheme is employed to evaluate the numerical flux across the faces. In addition to defining the discretized equations, the coefficient matrix Γ_p in the pseudotime term also introduces an artificial property procedure that allows the eigenvalues of the convergence process to be properly conditioned, thereby providing an efficient convergence algorithm to handle different time-scale problems. The introduction of the integral formulation for the discretized equation system allows the use of an arbitrary structured/unstructured grid capability to enable applications to complex geometry. Specific data and code structures are implemented in a fashion that mimics the conventional mathematical notations given previously and the corresponding operations for tensors, vectors, and scalar functions. To allow for different numbers of conservation equations in different problems, the number of equations is chosen at input. The spatial derivatives are discretized by a second-order-accurate upwind, finite volume process and solved by an approximate Riemann solver [12,13]. Representative results from this method are given in the following section.

IV. Simulation Results

To demonstrate the capability of the hyperbolic solution method for the Maxwell equations, we discuss numerical experiments where the Maxwell solver is applied in different situations. First, the diffusion of a magnetic field through a finite conductor in response to a step change in the magnetic field at the boundary is presented and compared with a corresponding analytical solution to demonstrate that the hyperbolic implementation produces accurate results for the diffusion problem. Following that, we contrast the approximate diffusion solution to a complete Maxwell solution for cases where the diffusivity is small enough that wave processes become important. We then look at the magnetic field propagation through a domain composed of a vacuum region enclosed by finite conducting walls. The results show excellent agreement between the numerical results of the present algorithm and the analytical solutions.

A. One-Dimensional Diffusion Problem

As an initial verification of the computational method, we consider the temporal evolution of the electric and magnetic fields in a one-dimensional semi-infinite domain, $0 \le x < \infty$. To enable comparison with an analytical solution, the displacement current term, $(1/c^2)\partial\mathbf{E}/\partial t$, is neglected so that the MHD equation applies. The corresponding electric field is then given by the curl of the magnetic field, $\mathbf{E} = (\nabla \times \mathbf{B})/\mu_0\sigma$. As the initial condition, the electric and magnetic fields are set to zero throughout the domain. At time zero, the boundary condition on the axial component of the magnetic field at $x = 0$ steps from $B_z = 0$ to $B_z = B_0$ and remains constant for all time. The other two magnetic field components at $x = 0$, and all three components as $x \to \infty$, remain unchanged. Under these conditions, the only nonzero components of the solution are the axial magnetic field B_z and the transverse electric field E_y. The MHD equation therefore reduces to a one-dimensional equation that possesses the similarity solution:

$$B_z = B_0\left\{1 - \text{erf}\left(\frac{x}{2}\sqrt{\frac{\mu_0\sigma}{t}}\right)\right\}, \qquad B_x = B_y = 0 \tag{53}$$

$$E_y = \frac{1}{\mu_0\sigma}\frac{\partial B_x}{\partial x} = \sqrt{\frac{1}{\pi\mu_0\sigma t}}\exp\left(\frac{x}{2}\sqrt{\frac{\mu_0\sigma}{t}}\right), \qquad E_x = E_z = 0 \tag{54}$$

where the error function is defined as

$$\text{erf}\,(z) = \frac{2}{\sqrt{\pi}}\int_0^Z e^{-u^2}\,du$$

.

For the numerical solution to this pure diffusion problem, we use the hyperbolic time-marching procedure presented earlier in the paper. For this first example, we drop the physical displacement current in Ampere's law so that Maxwell's equations simplify to the MHD equations, but they retain the pseudodisplacement current in pseudotime to demonstrate that the hyperbolic method provides an accurate and efficient solution in the purely diffusive limit. The numerical results are obtained on a two-dimensional uniform grid of the size 176×105 for the finite domain $0 \le x \le 50$ mm, $0 \le y \le 15$ mm with boundary conditions $B_z = B_0$, $\partial E_y/\partial x = 0$ on $x = 0$, along with a zero-slope condition, $\partial\mathbf{B}/\partial n = \partial\mathbf{E}/\partial n = 0$, on the remaining three sides. Applying a zero-slope condition at a finite location, $x = 50$, is slightly inconsistent with the analytical solution for which the magnetic field was set to zero as $x \to \infty$, but it is sufficient to allow detailed verification of the numerical results. The initial condition is $\mathbf{B} = \mathbf{E} = 0$. The properties of the medium are chosen as $\sigma = 10^{-2}$ mho/m. The time step is selected by setting the von Neumann number as $\Delta t/(\mu_0\sigma\Delta x^2) = 2.4$, yielding time step sizes of 1 ps. Comparisons with the one-dimensional analytical solution are presented in Fig. 1, where we show the field variation along the centerline of the two-dimensional domain. The results show very good agreement between the numerical and analytical solutions, apart from the anticipated error near the downstream boundary ($x = 50$) where the two boundary conditions are dissimilar. Parametric solutions of this example show the wave diffusion speed is inversely proportional to the electrical conductivity σ.

B. Magnetic Diffusion with Finite Displacement Current

We next repeat the $\sigma = 10^{-2}$ mho/m calculation with the displacement current term, $(1/c^2)\partial\mathbf{E}/\partial t$, included. When the displacement current is included, Maxwell's equations for this problem simplify to the telegraph equation for which the solution is composed of a precursor lossless wave followed by a residual diffusion wave that is left behind and decays exponentially with time after the initial pulse passes through. Similar characteristics are seen for the $\sigma = 10^{-2}$ mho/m calculation in Fig. 2 when the displacement current is included. The initial portion of the B field that propagates through the region is composed of a wave front that is immediately followed by a diffusion process. Consequently, the nature of the transient B field is completely different when displacement current effects are included. The analytical diffusion solution from Eq. (54) is shown in gray for reference. It can be seen from Fig. 2a that the magnetic field gradient and, therefore, the current density are considerably larger than in the diffusion case. Thus, the $J \times B$ force will be larger and can have a significant effect on the subsequent evolution of the fluid motion. Figure 2b also indicates that the diffusion model predicts considerably larger electric fields, especially at early times. This could have a significant effect, particularly for the modeling of fast opening switches. The numerical experiments indicate that, for the present problem, the displacement current affects the electromagnetic wave when the electrical conductivity of the media falls below approximately 1 mho/m. Under such conditions, the MHD assumption of a highly conductive plasma is not accurate, and the full Maxwell equation solver is necessary. The corresponding displacement current plot is given in Fig. 3, where the wavelike nature of propagation at early times is clearly evident.

C. Transient Propagation of Current Through Insulator/Conductor Region

The next case considers the transient electromagnetic field in the annular vacuum chamber, shown on the plot on the left of Fig. 4a that

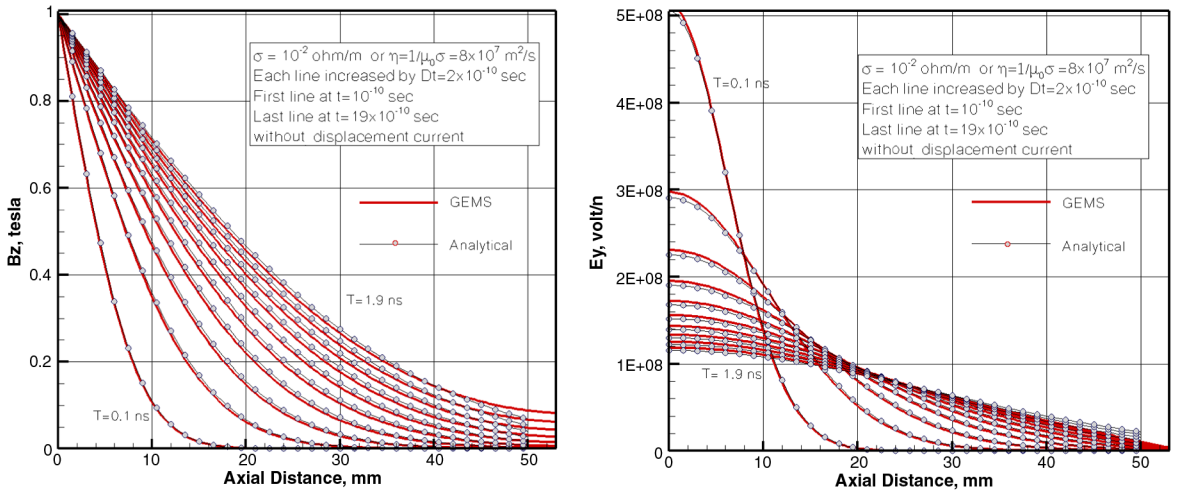

Fig. 1 Comparison of numerical solution (GEMS) of the first-order form of the MHD equations and analytical solution for $\sigma = 10^{-2}$ mho/m: a) magnetic field B_z and b) electric field E_y.

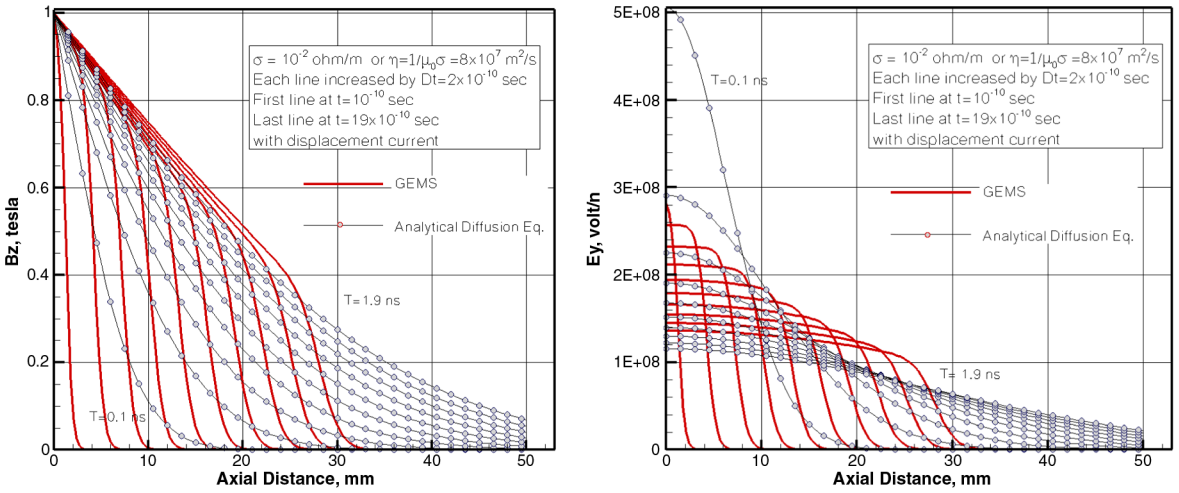

Fig. 2 Comparison of numerical field solution with displacement current included (solid lines) and with diffusion equation solution (dotted lines) for $\sigma = 10^{-2}$ mho/m: a) B_z and b) E_y.

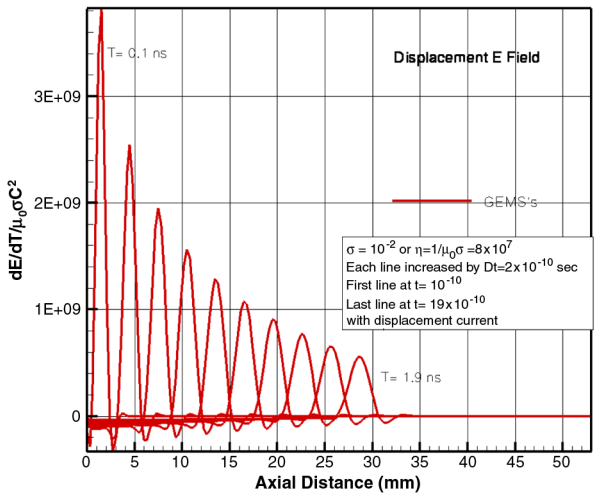

Fig. 3 Axial variation of displacement current at various times; $\sigma = 0.01$.

represents a simplified version of the pulsed plasma thruster (PPT) configuration. The length L of the vacuum region is 50 mm, while the inner and outer walls are formed by concentric, stainless steel cylinders of radii $r_1 = 22$ mm and $r_2 = 53$ mm, with a wall thickness of $\delta = 3$ mm, as shown in Fig. 4a. In place of the slug of plasma that serves as the propellant, the top of this annular region is enclosed by a solid stainless steel armature that carries the current from the inner to the outer electrode. As noted previously, the difficulty in this electromagnetic calculation is that the magnetic field must be carried by wave processes in the vacuum region, whereas in the stainless steel, it is carried by diffusion. Hence, the solution of the complete problem requires the capability for solving both the diffusion limit and the wave propagation limit simultaneously.

As a first step in addressing this problem, we begin by dropping the displacement current term in Maxwell's equations and filling the vacuum region with a fixed massless ether medium of finite conductivity so that both the stainless steel and vacuum regions can be represented by the diffusion approximation. This allows us to verify that the hyperbolic solution method presented here provides the same results as the solution of the more traditional MHD equation that is obtained from MACH2. Because MACH2 is an MHD code that deals only with the MHD equation, it cannot solve the present

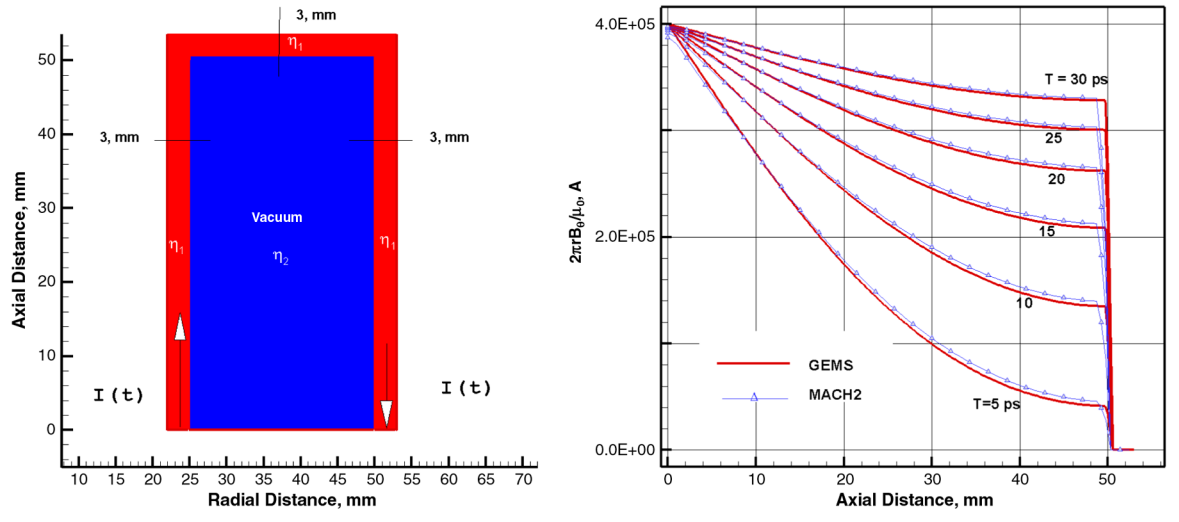

Fig. 4 Transient propagation of current through insulator/conductor region: a) geometry of concentric stainless steel channels with low-conductivity material, shown in black, replacing vacuum region in the center and by high-conductivity material (stainless steel) shown in gray; and b) comparison of transient magnetic field propagation as computed by GEMS (solid lines) and MACH2 (dotted lines).

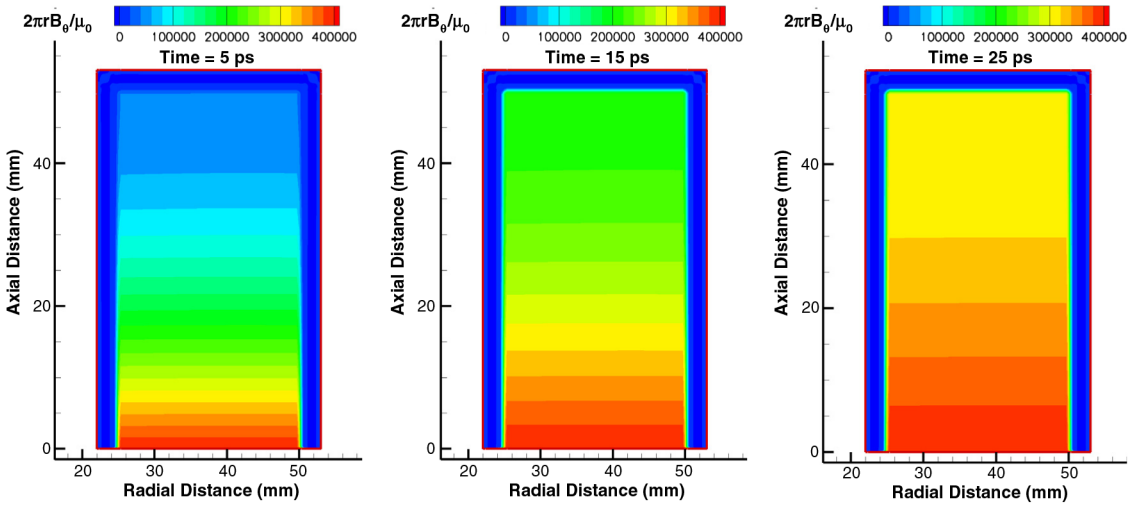

Fig. 5 Transient current distribution in ether region surrounded by stainless steel obtained with diffusion equation: a) 5, b) 15, and c) 25 ps.

problem unless the vacuum region has a finite electrical conductivity to propagate the magnetic field by diffusion [14]. Following this diffusion calculation, we then reintroduce the displacement current effects in the Maxwell equations and recompute the solution with the conductivity in the vacuum set identically to zero to contrast the differences in the transient fields when they are propagated by displacement current rather than by the conduction current introduced by artificially augmenting the electrical conductivity of the medium.

For the ether solution, we set the electrical conductivity in the vacuum region to $\sigma = 10^{-2}$ mho/m and specify the conductivity of the stainless steel walls as $\sigma = 8 \times 10^{5}$ mho/m. The time step for the diffusion calculation is set at $\Delta t = 0.1$ ps to catch the very fast initial wave diffusion phenomena in the vacuum (ether) region. Figure 4b compares the axial distribution of the current flow (the rB_θ field) as a function of axial distance for six different times, as predicted by GEMS and MACH2. The field is seen to propagate through the ether in exponential-like fashion. The very high conductivity in the stainless steel wall on the end of the domain, as compared with the ether, causes the slope of the curves to change discontinuously and to decay very rapidly to zero. On these very short time scales, the current diffuses to only a very thin skin depth in the stainless steel. The close agreement between the GEMS and MACH2 results is further evidence that the wavelike computational scheme in GEMS provides accurate solutions to problems involving pure diffusion.

Contour plots of the rB_θ field for this same case taken from the GEMS solution are presented in Fig. 5 for three time instants (5, 15, and 25 ps). These contour plots indicate that the current flow (the rB_θ field) in the ether is essentially one dimensional, with the only two-dimensional effects occurring in the skin effect region inside the stainless steel walls on the sides of the low-conductivity region. The grids used in the stainless steel are not sufficiently refined to represent this skin effect accurately, but the plots show that the diffusion depth into the stainless steel is very small. At much longer times (results not shown), the entire current diffuses into the stainless steel, and none of the current is carried by the low-conductivity ether.

Companion calculations of the same geometry with the displacement current term, $(1/c^2)\partial \mathbf{E}/\partial t$, included and the conductivity in the vacuum region set to zero are presented in Figs. 6 and 7. Figure 6 compares the displacement current calculations (full Maxwell solutions) with the diffusion current solution (conduction current only, no displacement current) previously shown in Fig. 5b. As can be seen, there are significant differences between magnetic field propagation by diffusion and by wave processes. When the conductivity is zero, Maxwell's equations reduce to a pure wave equation, and disturbances are carried by a wave moving at the (constant) speed of light. By contrast, the speed of the diffusion wave is proportional to the electrical diffusivity and decreases as the inverse square root of time. Furthermore, the amplitude of the diffusion wave is damped exponentially, while the pure wave propagating through the lossless medium maintains constant amplitude. For the ether conductivity value chosen here ($\sigma = 10^{-2}$ mho/m), the diffusion process propagates considerably faster than the speed of light, and so it reaches the end of the domain before the wave solution. (Setting the conductivity to 10^{-2} mho/m is arbitrary, and an ether conductivity could be chosen to more closely match the speed of the wave solution, but no attempt to do so has been made here.)

The qualitative character of the two families of rB_θ-field lines is also different. The field lines are concave downward for the wave solution, while they are concave upward for the diffusion solution, a further reflection that the two physical mechanisms of transport are based upon completely different physics. These numerical results demonstrate the importance of a solution technique that handles all regimes of operation.

Representative contour plots of the rB_θ field at three different times are given in Fig. 7 for the case in which the field is transported by the displacement current. These solutions are at the same times as those in Fig. 5 and give a direct comparison of the impact of the two methods of propagating magnetic field. It is important to note that the parameter, $2\pi rB_\theta/\mu_0$, represents the sum of both the conduction current and the displacement current. In Fig. 5, the displacement current is zero (the $\partial \mathbf{E}/\partial t$ term is omitted), while in Fig. 7, the conduction current vanishes in the vacuum region (where the

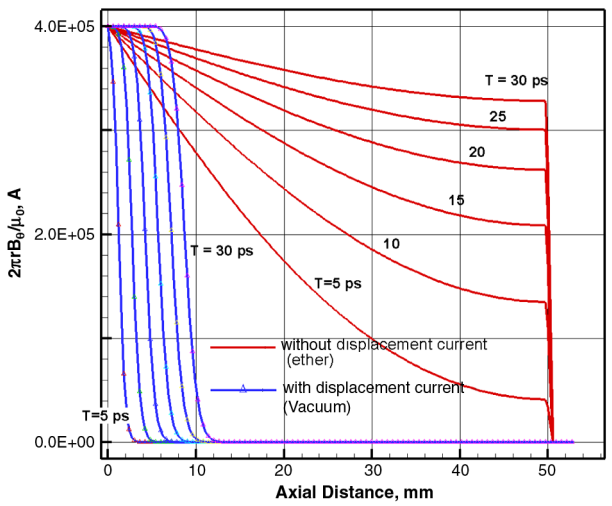

Fig. 6 Comparison of displacement current in vacuum with simulated physical current in ether medium.

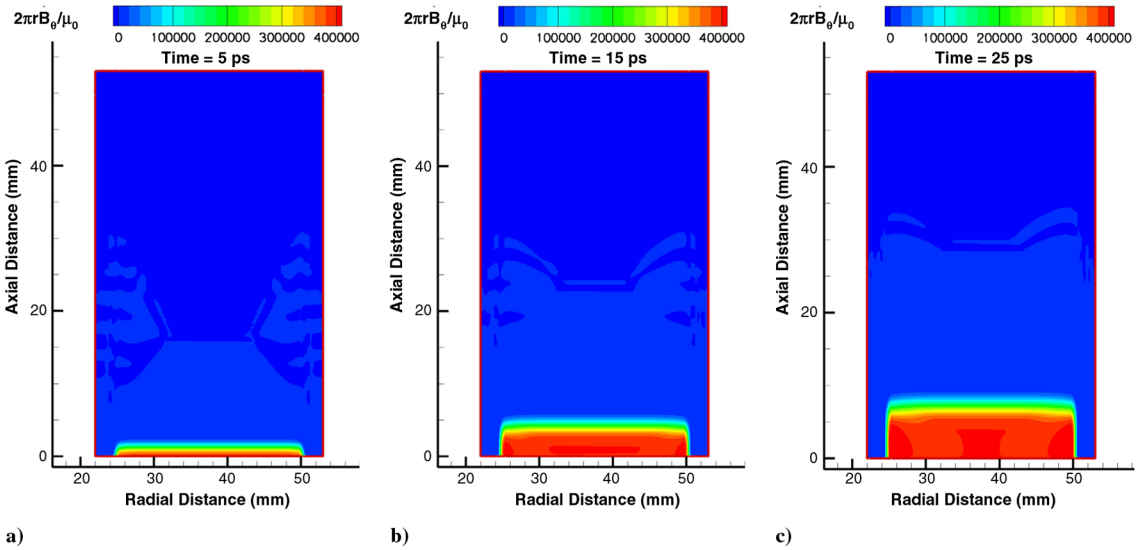

Fig. 7 Transient current distribution in vacuum region surrounded by stainless steel as a function of time: a) 5, b) 15, and c) 25 ps. Solutions obtained with Maxwell equations including displacement current term.

conductivity is zero). The wave solution shown in Fig. 7 does include current along that portion of the electrodes over which the magnetic wave has passed, but it is zero in front of it. By contrast, the surface current on the stainless steel in the diffusion solutions goes all the way around the closed circuit, starting from time zero but with an exponentially small amplitude that increases with time until a final uniform current is established.

The previously mentioned diffusion and Maxwell solutions show major differences on a picosecond time scale, but many of the key physics in PPT simulations occur on a microsecond time scale. It is important to ascertain whether any of these early time differences remain at later times or whether additional displacement current effects are introduced during the PPT cycle. Specific answers to these questions require detailed simulations of the entire pulse phenomena and careful comparisons with the companion experiments. As a first comparison of the two solutions at longer times, we present here some longer time simulations of the displacement current case for the present simplified problem. Clearly, at infinite time, both the wave solution and the diffusion solution will approach the same steady-state condition with a uniform magnetic field, zero current in the vacuum region, a linear magnetic field, and uniform current density in the stainless steel. (The steady-state diffusion solution will have a minute current in the vacuum region, determined by the ratios of the conductivities in the stainless steel and ether.) The results in Fig. 5 can easily be extrapolated to steady conditions, whereas the wave solutions in Fig. 7 are so early in time that the approach to steady state cannot be anticipated.

To address this issue, we present some longer time solutions in Fig. 8, which shows the time history value of the total current at a point near the center of the vacuum region (the precise location is indicated in the inset). The figure contains five curves. One of the five gives the solution based on pure diffusion with the conductivity in the ether set to $\sigma = 10^{-2}$. The remaining four solutions are for wave propagation in the vacuum region, with the surrounding conductor set to four different values of conductivity of $\sigma = 8$, 800, 8000, and 800,000, respectively. The diffusion solution results in a monotonic increase in the total current as a function of time as the magnetic field diffuses into the ether with no indication of wave motion. The four wave solutions all show a damped wavelike character for which the rate of damping decreases as the conductivity of the surrounding metal is increased. Physically, the wave reverberates throughout the vacuum region, reflecting from the walls, but at each reflection, a small portion of the wave is absorbed into the surrounding conductor. As the conductivity of the conductor is increased, the fraction of the incident wave that is absorbed decreases (the higher the conductivity, the slower the magnetic field diffuses into the conductor), and the wave decays more slowly. This example clearly shows the capability of solving wavelike phenomena (in the vacuum region) in conjunction with diffusion phenomena (in the surrounding walls) using a common hyperbolic solver.

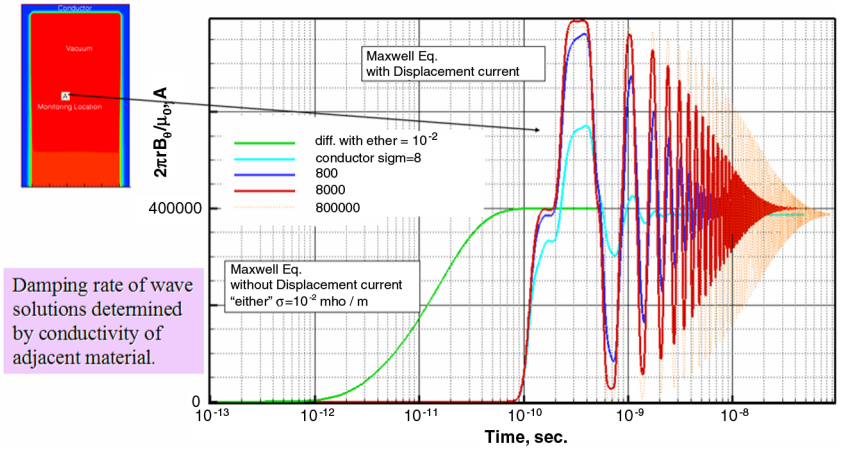

Fig. 8 Time history of Maxwell equation solutions with and without displacement current.

V. Conclusions

A new numerical procedure for computing electromagnetic fields that are closely coupled to fluid dynamic phenomena is presented. The method is aimed at those applications where the MHD approximation is valid over portions of the computational domain but for which there remain finite zones where the effects of displacement current dominate and the full Maxwell equations must be solved. Rather than combining the equations to form a second-order MHD equation, as is generally done in MHD solution techniques, the full Maxwell equations are retained in their first-order form. To deal efficiently with regions in which the displacement current is small, causing the system to become stiff, the first-order set is embedded in pseudotime using an artificial speed of light that keeps the equations well ordered in all domains, allowing classical hyperbolic numerical solution techniques to be applied accurately and efficiently over the complete spectrum from the wave propagation limit to the diffusion limit. Before coupling with the equations of fluid dynamics, the Lorentz force and the ohmic heating terms are transformed to conservation form by means of the Poynting vector and a magnetic energy density term, eliminating all source terms from the combined fluids/electromagnetic system except for the current density in Ampere's law. The method has advantages in that its first-order form, which is directly analogous to the first-order character of the fluid equations, makes the coupling between fluids and electromagnetics very straightforward. In addition, because the electric field is computed directly from its own equation rather than being determined by differentiating the magnetic field, as is done in methods that solve the MHD equation, it gives more accurate electric field solutions.

To demonstrate the capability of the new algorithm for both the full Maxwell equations and the MHD approximation, numerical experiments are presented in which the algorithm is applied in two different situations. The first case concerns the diffusion of a magnetic field through a finite conductor in response to a step change in the magnetic field at the boundary. This pure diffusion problem is solved by the hyperbolic technique and compared with a closed-form analytical solution to demonstrate the capability of the numerical procedure in this extreme limit. Comparisons between the numerical and analytical solutions indicate very good agreement and also show that the wave diffusion speed is proportional to the electrical diffusivity.

The second case involved comparisons of the approximate diffusion solution to the complete Maxwell equations for cases where the diffusivity is small enough that wave processes becomes important. Here, the algorithm was exercised for two different conditions. In the first case, the effects of the displacement current were ignored, the hyperbolic solution method was used, and the results were compared with calculations done with the MACH2 MHD code. Again the comparisons were excellent, indicating the method is applicable in the MHD regime. This same problem was then solved with the displacement current retained in the equations to demonstrate the dramatic impact it can have on the propagation of magnetic field. The line of demarcation between regimes below which the displacement current is important for this particular example was shown to correspond to lie in the regime in which the conductivity is below approximately 1 mho/m. Under such conditions, the MHD assumption of large conductivity is not accurate, and the full Maxwell equation solver is necessary.

These examples show that the first-order hyperbolic solution algorithm for the coupled Maxwell equations and fluid motion equations provides a more accurate approach for the analysis of many interesting complex physical problems in which both real and displacement currents play significant roles.

Acknowledgment

This work was partially supported by the Arnold Engineering and Development Center under contract F40600-00-D-001 0024.

References

[1] Moeller, T., Keefer, D., and Rhodes, R., "Experimental Pulsed Plasma Thruster for Code Evaluation," *31st IEEE International Conference on Plasma Science*, IEEE Publ., Piscataway, NJ , 2004, p. 302.

[2] Powell, K. G., Roe, P. L., Myong, R. S., Gombosi, T., and De Zeeuw, D. L., "An Upwind Scheme for Magnetohydrodynamics," 12th AIAA CFD Meeting, AIAA Paper 1995-1704, June 1995.

[3] Li, D., Keefer, D., Rhodes, R., Merkle, C. L., and Thibodeaux, R., "Analysis of MHD Generator Power Generation," *Journal of Propulsion and Power*, Vol. 21, No. 3, 2005, pp. 424–432. doi:10.2514/1.4415

[4] Bunde, R., Muntendbruch, H., Raeder, J., Volk, R., and Zankl, G., *MHD Power Generation: Selected Problems of Combustion MHD Generators*, Springer–Verlag, New York, 1975.

[5] Felderman, E. J., Chapman, R., Jacocks, J. L., Horn, D. D., and Bruce, W. E., III, "High-Pressure Arc Heater Development and Modeling: Status and Requirements," *Journal of Propulsion and Power*, Vol. 12, No. 6, Nov.–Dec. 1996, pp. 1044–1052. doi:10.2514/3.24142

[6] Keefer, D., and Rhodes, R., "Numerical MHD Simulations of the DECADE Plasma Opening Switch Using MACH2," *IEEE International Conference on Plasma Science*, IEEE Publ., Piscataway, NJ, 1996, p. 299.

[7] Smith, L. M., Keefer, D. R., and Wright, N. W., "Interferometric Investigation of a Cablegun Plasma Injector," *IEEE Transactions on Plasma Science*, Vol. 28, No. 6, Dec. 2000, pp. 2272–2275. doi:10.1109/27.902256

[8] Burton, R. L., and Turchi, P. J., "Pulsed Plasma Thruster," *Journal of Propulsion and Power*, Vol. 14, No. 5, 1998, pp. 716–735. doi:10.2514/2.5334

[9] Cramer Kenneth, R., and Pai Shih-I, *Magnetofluid Dynamics for Engineers and Applied Physicists*, Scripta, Washington, D. C., 1973.

[10] Rooney, D., Moeller, T., Keefer, D., Rhodes, R., and Merkle, C., "Experimental and Computer Simulation Studies of a Pulsed Plasma Accelerator," 2007 Joint Propulsion Conference, AIAA Paper 2007-5225, July 2007.

[11] Munz, C. D., Ommes, P., and Schneider, R., "A Three-Dimensional Finite-Volume Solver for the Maxwell Equations with Divergence Cleaning on Unstructured Meshes," *Computer Physics Communications*, Vol. 130, Nos. 1–2, 2000, pp. 83–117. doi:10.1016/S0010-4655(00)00045-X

[12] Li, D., Venkateswaran, S., Lindau, J., and Merkle, C. L., "A Unified Computational Formulation for Multi-Component and Multi-Phase Flows," 43rd AIAA Aerospace Sciences Meeting and Exhibit, AIAA Paper 2005-24906, Jan. 2005.

[13] Li, D., Xia, G. P., Sankaran, V., and Merkle, C. L., "Computational Framework for Complex Fluid Physics Applications," *Computational Fluid Dynamics 2004: Proceedings of the Third International Conference on Computational Fluid Dynamics, ICCFD$_3$, Toronto, 12–16 July 2004*, edited by C. Groth, and D. W. Zingg, Springer–Verlag, Berlin, 2004, pp. 619–624.

[14] Peterkin, R. E., Frese, M. H., and Sovenec, C. R., "Transport Of Magnetic Flux in an Arbitrary Coordinate Ale Code," *Journal of Computational Physics*, Vol. 140, No. 1, 1998, pp. 148–171. doi:10.1006/jcph.1998.5880

W. Anderson
Associate Editor